Applied Geochemistry 123 (2020) 104820

Contents lists available at ScienceDirect

Applied Geochemistry

journal homepage: http://www.elsevier.com/locate/apgeochem

Unraveling groundwater functioning and nitrate attenuation in evaporitic karst systems from southern Spain: An isotopic approach

Nicolas Valiente [a,b,*], José Manuel Gil-Márquez [c], Juan José Gómez-Alday [b], Bartolomé Andreo [c]

[a] Centre for Biogeochemistry in the Anthropocene, Department of Biosciences, Section for Aquatic Biology and Toxicology, University of Oslo, PO Box 1066, Blindern, 0316, Oslo, Norway
[b] Biotechnology and Natural Resources Section, Institute for Regional Development (IDR), University of Castilla–La Mancha (UCLM), Campus Universitario s/n, 02071, Albacete, Spain
[c] Department of Geology and Center of Hydrogeology of the University of Málaga, Faculty of Science, 29071, Málaga, Spain

ARTICLE INFO

Editorial handling by Prof. M. Kersten

Keywords:
Brine groundwater
Stable isotopes
Evaporitic karst aquifer
Solute transport
Nitrate attenuation

ABSTRACT

High evaporation rates in semi-arid to arid regions result in an increase in salinity that can exacerbate the effect of pollutants in water bodies.This study examines how groundwater drives pollution removal in wetlands, wells and springs within the Chaotic Subbetic Complexes (southern Spain). This evaporitic system, localy with a clear karstic functioning, is characterized by groundwater with a wide range of mineralization. Hydrochemical and multi-isotopic ($\delta^{34}S$, $\delta^{18}O$, $\delta^{15}N$, $\delta^{13}C$ and $\delta^{2}H$) techniques were used to understand the geochemical processes leading to pollutant attenuation within the complexes. There, regional groundwater evolve from recharge/transition areas, with low salinity, to the discharge zone. Mineralization of groundwater depends on the dissolution of evaporitic deposits (gypsum, halite) of Keuper age, which increases salinity of the water drained by the outlet springs. $\delta^{15}N$ and $\delta^{18}O$ values of dissolved nitrate (NO_3^-) were used to estimate the relative contribution of N sources. NO_3^- is mainly derived from agricultural inputs (nitrate and urea fertilizers). Long-residence groundwater plays an important role in the biogeochemical evolution. Denitrification is responsible for NO_3^- removal in transitional zones and discharge springs. This process is promoted by the oxidation of organic carbon, derived from recharge areas and further transported to deeper zones of the aquifer. The findings of this study provide a new understanding of how hydrogeological functioning is connected to pollutant removal in an evaporitic karst system, where the scale of groundwater flows plays a key role in biogeochemical processes.

1. Introduction

Through inputs of agricultural and farming wastes, which include pesticides and drugs, and both organic and inorganic wastes from domestic and industrial sources (e.g., Dodds, 2006; Destouni and Darracq, 2009; Bhagowati and Ahamad, 2019; Boyd, 2020), the excess in anthropogenic loading of nutrients derives in eutrophication of aquatic ecosystems, including wetlands (Lowe and Keenan, 1997; Smolders et al., 2010; Serrano et al., 2017). Despite nitrogen (N) is an essential nutrient for all organisms, the invention of technical N-fixation through the Haber–Bosch process led to drastically modified the global N budget in aquatic environments (Canfield et al., 2010). The European Groundwater Directive (EC, 2006) considers nitrate (NO_3^-) as priority substance due to its negative effects on health (Comly, 1945; Fraser and Chilvers, 1981; Ward et al., 2005) and on the eutrophication of surface water bodies (Dassenakis et al., 1998; Kraft and Stites, 2003). For human water supplies, the NO_3^- concentration threshold established by Directive 98/83/CE (EC, 1998) is 50 mg/L.

While wetland pollution is a worldwide problem related to anthropogenic activities, several studies have shown the potential of wetlands to improve water quality by removing compounds such as phosphate (PO_4^{3-}) or NO_3^- (Nichols, 1983; Baker, 1998; Fischer and Acreman, 2004; Gilbert et al., 2014; Gómez-Alday et al., 2014; Más-Pla and Menció, 2019). Removal of NO_3^- in wetlands depends on reduction-oxidation (redox) reactions which follow a sequence on the basis of thermodynamic principles (Stumm and Morgan, 1981). It starts using oxygen (O_2) as electron acceptor, followed by NO_3^-, manganese (Mn) and iron (Fe) oxides, sulfate (SO_4^{2-}) and carbon dioxide (CO_2). Redox pathways that

* Corresponding author. Centre for Biogeochemistry in the Anthropocene, Department of Biosciences, Section for Aquatic Biology and Toxicology, University of Oslo, PO Box 1066, Blindern, 0316, Oslo, Norway.
E-mail address: n.v.parra@ibv.uio.no (N. Valiente).

https://doi.org/10.1016/j.apgeochem.2020.104820
Received 27 February 2020; Received in revised form 31 October 2020; Accepted 2 November 2020
Available online 5 November 2020

are significant in pollution mitigation include multiple microbially-mediated reactions. Denitrification (heterotrophic or autotrophic) is the dominant process that removes NO_3^- from groundwater. Dissimilatory nitrate reduction to ammonium (DNRA) involves the transformation of NO_3^- to ammonium (NH_4^+). Dissimilatory bacterial sulfate-reduction (BSR) yields energy for sulfate-reducing microbes under anaerobic conditions. Methanogenesis involves the biological decomposition of carbon biomass in the absence of oxygen.

In arid and semi-arid regions, where high evaporation rates are typical, the accumulation of solutes can lead to an increase in salinity, which enhances the toxicity of certain chemicals to aquatic biota due to either chemical (bioavailability) or biological (physiological) factors (Hall and Anderson, 1995). Regarding NO_3^-, the main risk is associated to environmental conditions typical from these regions (e.g. low precipitation, high evaporation) which result biomagnication effects compared to freshwater systems (Williams, 2002). Nevertheless, recent studies suggest that saline wetlands can recycle nutrients more efficiently than freshwater systems (Santoro, 2010; Wurtsbaugh et al., 2017; and reference therein). The Andalusia region, located in the south of Spain, is a favorable area for the formation of saline wetlands due to its hydroclimatic and geological conditions. The abundant wetlands linked to the geological unit known as the Chaotic Subbetic Complexes (CSC) present a wide range of salinity, hydrochemical facies, and hydroperiod, resulting from the interaction of wetlands and groundwater (Andreo et al., 2016), showing a similar interaction than the observed in the Prairie potholes (Mills et al., 2011). Moreover, dissolution processes (karstification) affect evaporitic rocks in the CSC, contributing to the development of secondary porosity and permeability, resulting in the formation of exokarst features. In addition, the dissolution of evaporites promotes an increase in salinity. Together with saline wetlands, brine springs are commonly found in the CSC because they partially drain groundwater brought by regional groundwater flowpaths of long residence time (10,000–100,000 years), which are highly geochemically evolved (Gil-Márquez et al., 2017a, 2020).

Amarga and Jarales (Córdoba Province), as well as Brujuelo (Jaén Province) wetlands have been selected in this study as representative wetlands in the region. While these wetlands are protected as Natural Reserves by the Andalusian administration and included in the Ramsar list, a significant agricultural impact is observed in the studied areas. The usual agricultural practices in the region include plowing and fertilization, which produce siltation of wetlands due to sedimentation (Rodríguez-Rodríguez et al., 2009) and water pollution (Novales et al., 1991). The resulting high concentrations of NO_3^- and NO_2^- have been occasionally documented in the water of CSC wetlands, as well as associated to brine groundwater drained by springs (Gil-Márquez, 2018).

The identification of pollution sources and mitigation pathways can be achieved by the determination of stable isotopes ($\delta^{13}C$, $\delta^{15}N$, $\delta^{18}O$, $\delta^{34}S$) coupled to hydrochemistry. Previous studies in aquatic ecosystems have involved multi-isotope approaches to identify NO_3^- and SO_4^{2-} sources (Vitòria et al., 2004; Kendall et al., 2008) and reveal biogeochemical turnover through bacterial-mediated redox reactions (Puig et al., 2013; Hosono et al., 2014; Caschetto et al., 2017; Valiente et al., 2018; Margalef-Marti et al., 2019). Stable isotopes of the water molecule ($\delta^{18}O_{H2O}$ and $\delta^{2}H_{H2O}$) can be also used as tracers to obtain information about hydrogeological processes (e.g. precipitation, evaporation, groundwater recharge) to be taken into account when studying attenuation processes in aquatic ecosystems (Barnes and Allison, 1988; Kendall and McDonnell, 2012; Jambrina-Enríquez et al., 2018).

In this study, we use stable isotopes ($\delta^{2}H$, $\delta^{15}N$, $\delta^{18}O$ and $\delta^{34}S$) in combination with major ion hydrochemistry to understand the biogeochemical processes leading to pollutant attenuation within the CSC (Spain). There, saline groundwater and brackish wetlands are connected (Andreo et al., 2016). We examine potential of pollution sources and microbially-mediated redox reactions in the study area. While stable isotopes in pollution assessment studies of karst aquifers have been widely used (Katz et al., 2004; Barbieri et al., 2005; Li et al., 2008; Albertin et al., 2012; Gammons et al., 2013), the application of isotopic approaches in evaporitic karst systems is limited to low salinity groundwaters (Panno et al., 2001; Einsiedl et al., 2009; Urresti-Estala et al., 2015; González-Ramón et al., 2017; Ayadi et al., 2018; Egbi et al., 2018). The results of this study will help understand the attenuation processes of pollutants (i.e. nitrate) in saline groundwater with long residence times, providing new insights into agricultural management and protection strategies for evaporitic karst systems.

2. Study areas

The CSC (Fig. 1A) extend in a broad band of 300 km-length, of NE-SW direction, and is flanked by the northern border of the Betic Cordillera and the Guadalquivir River basin (Vera and Martín-Algarra, 2004). The CSC are mainly formed by Upper Triassic rocks, including multicolored clays and evaporite rocks (gypsum, halite), although blocks of other lithologies and ages are also present: sandstones, marls, ophites, limestones, and dolostones from Triassic to Miocene ages. Gypsum is present as massive bodies, but also in polygenic breccias. Halite is absent at the surface, but is present at depth as determined through groundwater hydrochemistry and some boreholes drilled in CSC outcrops (Carrasco, 1986; Calaforra and Pulido-Bosch, 1999). The whole set of rocks is highly folded and brecciated, as a result of their gravitational displacement during the Alpine orogeny, in the lower and mid-Miocene (Rodríguez-Fernández et al., 2013). Consequently, the CSC present a disorganized and chaotic inner structure, and are a megabreccia with a clayey-evaporite matrix, in which olistoliths of different size and nature are embedded.

The hydrogeologic setting of the CSC is complex due to the lithological heterogeneity of the media (Andreo et al., 2016). Owing the poorly conductive nature of most of the materials forming this unit, groundwater flow is attenuated and diffused. The karstification of evaporite rocks has resulted in the appearance of unstable karst cavities and conduits, leading to surface collapses and subsidence. As a consequence exokarst forms are shaped, including sinkholes and surface depressions (Calaforra and Pulido-Bosch, 1999; Gutiérrez et al., 2008). The karstification of evaporite rocks allows rapid hydrogeological connections via conduits (Gil-Márquez et al., 2017b). The Gravity-Driven Regional Groundwater Flow (GDRGF) described by Toth (1963, 1970) inspired Andreo et al. (2016) to develop a conceptual model that explains the general hydrogeological functioning of the CSC, as well as the hydrochemical and hydrological particularities of the spring and wetlands related to them. Therefore, wetlands at higher elevations are normally emplaced above the phreatic level and function as recharge areas. These waters generally have low salinity, as they have a meteoric origin or are connected with runoff or with sporadic local groundwater flows of short residence time. Outlets and wetlands located at lower elevations (discharge areas) are linked to long deep groundwater flows with increased residence time (Gil-Márquez et al., 2020), resulting in high salinity and relatively high temperature. Springs and wetlands in intermediate positions (transitional areas) have variable salinity, due to the heterogeneity of the media and the variable contribution of different groundwater flows of diverse path lengths and ages. A complete description of the sampling sites included in this study is shown in Fig. 1.

2.1. Jarales area

The Jarales area is located in the south of Cordoba Province, between Genil River (southwards) and Anzur River (northwards), and includes prominent outcropping of CSC (Fig. 1B). Climate is Mediterranean, defined by an extended summer dry season. The average annual rainfall is 508 mm, and the mean air temperature is 17.2 °C (Gil-Márquez, 2018). The prevailing lithologies are Triassic, mainly gypsum, marls and, to a lesser extent, sandstones (Martín-Serrano, 1986). These rocks have been subjected to extensive tectonic activity, forming a chaotic

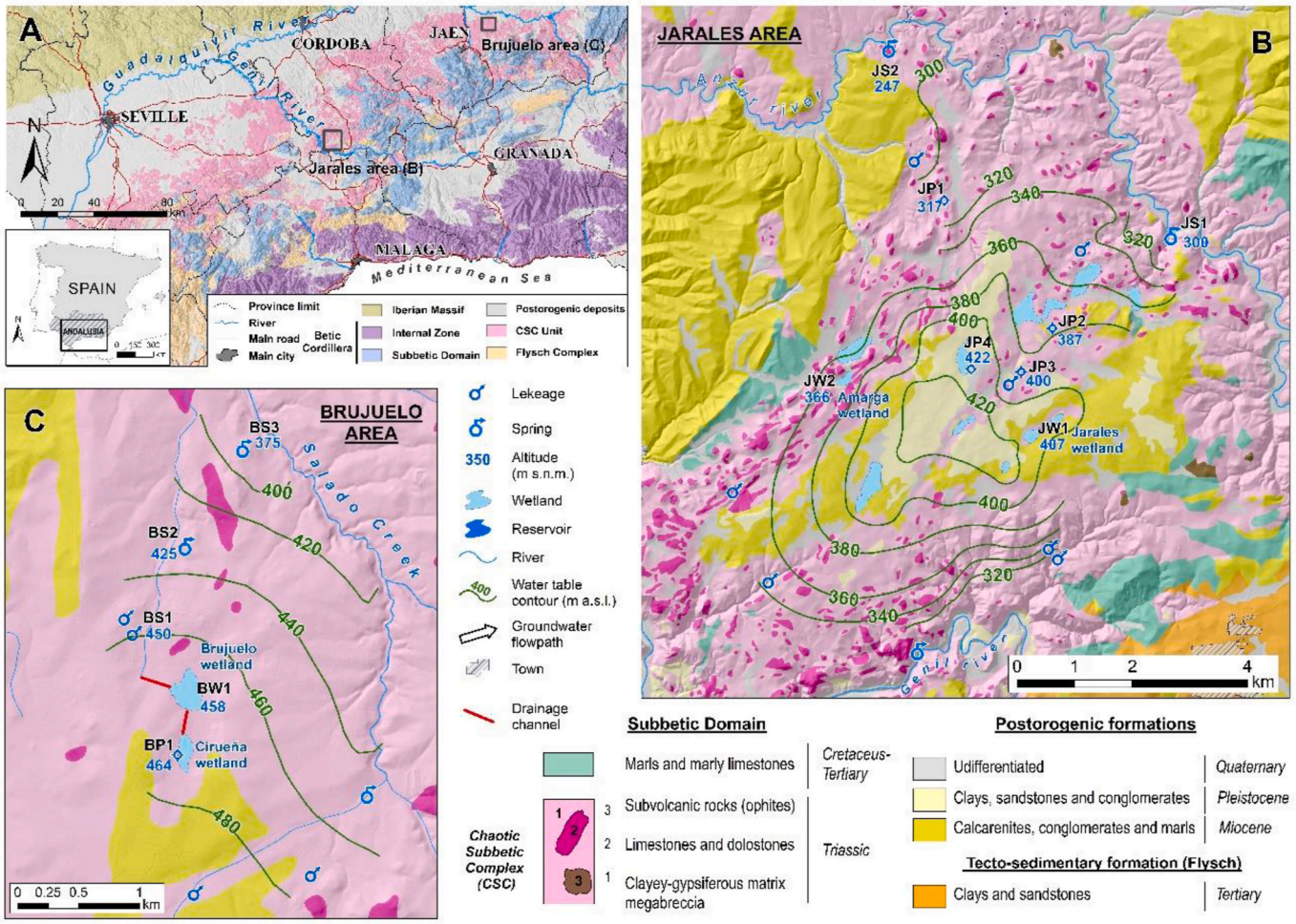

Fig. 1. Study area including A) Chaotic Subbetic Complexes (CSC) in the south of Spain; B) Jarales area; and C) Brujuelo area. Modified from Andreo et al. (2016) and Gil-Márquez et al. (2020).

mélange where blocks of carbonates, ophites, and massive gypsum are embedded. Conglomerates and marls of Miocene and Pleistocene ages discordantly outcrop above the CSC rocks. The geomorphology of the study area is as a plateau characterized by a smooth relief in its central part where karst endorheic depressions are fairly abundant. Wetlands of diverse characteristics are commonly found in those depressions. Northwards, karstic depressions impede the prolonged flooding of endorheic zones. According to the water table sketch of the area (Andreo et al., 2016, Fig. 1B), groundwater flows in a radial divergent way, from the central part of the plateau towards its borders. This fact, together with the positioning of wetlands respect to groundwater flowpaths, influences the hydrological functioning. Two major hydrological settings in the area are Jarales (JW1) and Amarga (JW2) wetlands. Jarales wetland (407 masl) has a seasonal hydroperiod as it does not have water in dry conditions. Recharge is primarlly through rainfall and runoff inputs, although its position in transitional areas allows minor groundwater inputs in high flow regimes (Gil-Márquez, 2018). On the contrary, Amarga wetland (366 masl) is a permanent wetland and it receives large

Table 1
Description of the sampling sites included in this study. P: precipitation (mm). T: temperature (°C). EC: electric conductivity (mS/cm). WTD: water table depth (m). Q: discharge rate (L/s). Height expressed as meters above sea level (masl). n: number of field observations. P, T, EC, WTD, and Q refer to mean values obtained from Gil-Márquez (2018). Mean values in wetlands come from monthly data, those in springs from fortnightly data, while those in wells were calculated from punctual data.

Area	P	Air T	Sampling site	Description	Type	Height	EC	WTD	Q	Water T	n
Jarales	508	17.2	JW1	wetland	Recharge/transition	407	3.1	-	-	18.8	15
			JW2	wetland	Recharge/transition	366	3.6	-	-	18.9	25
			JP1	well	Recharge/transition	317	-	6.1	-	-	-
			JP2	well	Recharge/transition	387	-	5.2	-	-	-
			JP3	well	Recharge/transition	400	8	2.7	-	18.8	4
			JP4	well	Recharge/transition	422	-	6.8	-	-	-
			JS1	spring	Discharge	300	45	-	5	20.6	77
			JS2	spring	Discharge	247	149	-	1	20.7	131
Brujuelo	511	17.7	BW1	wetland	Recharge/transition	463	12	-	-	17.8	16
			BP1	well	Recharge/transition	458	4.2	-	-	17.4	2
			BS1	spring	Recharge/transition	450	13	-	1	15.9	51
			BS2	spring	Discharge	425	121	-	-	19.2	55
			BS3	spring	Discharge	375	196	-	4	20.5	28

groundwater inputs all year. The groundwater discharge in the area is through three brine springs adjacent to the Anzur and Genil Rivers. The major outlets are Upper Anzur (JS1), to the east (300 masl), and Lower Anzur (JS2), to the north (247 masl), which are also included in the control points (Table 1).

2.2. Brujuelo area

Brujuelo is located in southern Jaen Province, in a plain area at the western margin of Salado Creek (Fig. 1C), a tributary of Guadalquivir River. Climate is also Mediterranean, with average values of rainfall and air temperature of 511 mm and 17.7 °C, respectively. The CSC in the Brujuelo area has a more olistrostomic nature, characterized by pebbles embedded in a sandy-clayey matrix, whose formation is related to debris flow processes (Roldán, 1995). Among them, there are blocks of gypsum, sandstones and, dolostones, which occasionally reach hundreds of meters of dimension. There are not abundant exokarst forms, except for two karst depressions that are occupied by Brujuelo (BW1) and Cirueña wetlands. These depressions are anthropogenically modified by drainage ditches that favor water evacuation from Cirueña towards Brujuelo wetland, and from there to a small creek to the east (Fig. 1C) via a tunnel. As a consequence, Cirueña wetland (463 masl) has ephemeral flooding, while Brujuelo wetland (458 masl) has a seasonal hydroperiod. Nevertheless, the groundwater table is very close to Cirueña wetland, and can be measured in a well (BP1) located in its bed (Table 1). The main discharge points of the system are some brine springs located by Salado stream. San Carlos spring (BS3) is the lowest outlet in the area (375 masl) and it drains the most saline water. The water table contour sketch (Fig. 1C) indicates that groundwater flows from the southwest of the area (where the wetlands are emplaced) towards Salado stream (Andreo et al., 2016). Thus, Cirueña is a recharge wetland, while Brujuelo wetland is located in a more transitional position. Towards San Carlos spring, there are other groundwater discharge points: BS1 (450 masl), a small outlet near the exit of the artificial drainage of Brujuelo wetland, and Brujuelo spring (BS2, 425 masl), a discharge point used for salt exploitation. A previous geochemical study performed in the area (Gil-Márquez et al., 2017a) suggests that the drainage of the system is defined by hierarchically sorted groundwater flowpaths. Those points located at lower positions are related to long flows of great residence time in the media, while wetlands and outlets in higher altitudes are linked to short groundwater flows. It was also deduced from isotope data that Brujuelo wetland receives groundwater inputs from Cirueña wetland, and part of the drainage of BS1 proceeds from water infiltrated in the first wetland (Gil-Márquez et al., 2017a).

3. Material and methods

3.1. Field survey

In May 2016, 15 samples were collected from different control points in Jarales "-J-" (n = 8) and Brujuelo "-B-" area (n = 5), including wetlands "-W-" (JW1, JW2, and BW1), wells "-P-" (JP1, JP2, JP3, JP4, and BP1), and springs "-S-" (JS1, JS2, BS1, BS2, and BS3) (Fig. 1, Table 1). Simultaneous measuring of physicochemical parameters was performed *in situ*. Water temperature (T) and electrical conductivity (EC) were measured with WTW conductivimeter-thermometer 3310, while pH, dissolved oxygen (DO) and redox potential (Eh) were made using a HACH HQ40d multimeter. Following the official standard methods (APHA, AVWA, 2012), water samples were refrigerated in the field and kept in darkness before further analysis.

The sampling campaign coincided with the third dry year in the period from 2013/14 to 2015/16 (Gil-Márquez, 2018). This dry period led to a significant decrease in the water stage of wetlands and the discharge rate of outlets. However, 56 mm and 53 mm of precipitation were measured in Brujuelo and Jarales areas, respectively, the fortnight before sampling, producing runoff inputs to the wetlands. As a result, JW1 was flooded after being dry for a few weeks.

3.2. Chemical analysis

Water samples for major ions were filtered with a 0.45 μm nylon Millipore® filter. For dissolved organic carbon (DOC) analysis, samples were filtered with a 0.20 μm nylon Millipore® filter. Major ion determinations were carried out in the laboratory of the Center of Hydrogeology of the University of Málaga (CEHIUMA). Alkalinity (as HCO_3^- + CO_3^{2-}) was determined by volumetric titration with 0.02 N H_2SO_4 to pH 8.3 (if pH of the sample was higher) for CO_3^{2-} quantification, and then to 4.45 for HCO_3^-. Major ions (Ca^{2+}, Mg^{2+}, Na^+, K^+, Cl^-, SO_4^{2-}) and Br^- measurements were made by ionic chromatography by using a METROHM Compact 930 IC flex for cations, and Compact 881 IC Pro for anions, with a 2% of precision and 0.1 mg/L of limit of detection (LOD) estimated from calibration standards. Due to the high salinity of the samples, they were diluted to 1 mS/cm before being introduced in the system. DOC concentration was determined by the high-temperature combustion method using a Shimadzu TOC-V Analyzer at the Servicios de Apoyo a la Investigación (SAI) of the University of A Coruña. Inorganic N-species were measured in the following 48 h after collection at the Institute for Regional Development (University of Castilla-La Mancha). NH_4^+ concentrations were quantified by UV-VIS spectrophotometry using the modified indophenol method, as described by Hood-Nowotny et al. (2010). Measurement of NO_2^- and NO_3^- concentration was achieved by UV-VIS spectrophotometry via the modified Griess reaction assay as described by García-Robledo et al. (2014). The precisions of NH_4^+ and NO_2^-/NO_3^- determination were, respectively, 2% and 4%. The LOD of such methods were 0.007 mg/L for NH_4^+ and 0.005 mg/L for NO_2^-/NO_3^-. Both were estimated from a set of standards.

3.3. Isotope analysis

Samples for stable isotopes were filtered as for major ions, by 0.45 μm, and shipped for further analysis. Isotope analyses included δ^2H and $\delta^{18}O$ of H_2O, $\delta^{34}S$ and $\delta^{18}O$ of SO_4^{2-}, $\delta^{15}N$ and $\delta^{18}O$ of NO_3^-, as well as $\delta^{13}C$ of DIC. δ^2H_{H2O} and $\delta^{18}O_{H2O}$ were measured using H_2 and CO_2 equilibrium techniques, respectively, following standard methods (Epstein and Mayeda, 1953), by dual inlet IRMS on a Finnigan MAT Delta S. For $\delta^{34}S_{SO4}$ and $\delta^{18}O_{SO4}$, dissolved sulfate was precipitated as $BaSO_4$ by adding 5% $BaCl_2{\cdot}2H_2O$ and HCl and boiling to prevent $BaCO_3$ precipitation (Dogramaci et al., 2001). The $\delta^{34}S$ was analyzed with a Carlo Erba EA-Finnigan Delta C IRMS. The $\delta^{18}O$ was analyzed in duplicate using a Thermo Quest high-temperature conversion elemental analyser (TC/EA) coupled in continuous flow with a Finnigan MAT Delta C IRMS. In the nitrate molecule, $\delta^{15}N_{NO3}$ and $\delta^{18}O_{NO3}$ were measured using a Cd-reduction method (McIlvin and Altabet, 2005; Ryabenko et al., 2009). In brief, NO_3^- was converted to NO_2^- through spongy cadmium reduction and then to nitrous oxide using sodium azide in an acetic acid buffer. Simultaneous $\delta^{15}N$ and $\delta^{18}O$ analysis of the N_2O produced was carried out using a Pre-Con (Thermo Scientific) coupled to a Finnigan MAT-253 Isotope Ratio Mass Spectrometer (IRMS, Thermo Scientific). The $\delta^{13}C_{DIC}$ was measured from filtered samples, further treated with ortho-phosphoric acid and shaken for 2 h to convert all HCO_3^- into CO_2 and reach equilibrium between phases(aqueous and gaseous), and the isotope ratio was measured in a Gas-Bench II coupled to a MAT-253 IRMS (Thermo Scientific).

Results are expressed in δ (‰) values relative to international standards: Vienna Standard Mean Ocean Water (V-SMOW) for $\delta^{18}O$ and δ^2H, Vienna Canyon del Diablo Troilite (V-CDT) for $\delta^{34}S$, atmospheric N_2 (AIR) for $\delta^{15}N$, and Vienna Pee Dee Belemnite (V-PDB) for $\delta^{13}C$. Analytical reproducibility of both international and internal reference samples of known isotopic composition was ±1‰ for δ^2H, ±0.3‰ for $\delta^{18}O_{H2O}$, ±0.2‰ for $\delta^{34}S$, ±0.5‰ for $\delta^{18}O_{SO4}$ and $\delta^{18}O_{NO3}$, and ±0.3‰ for $\delta^{15}N$ and $\delta^{13}C$, estimated using standard deviations from the duplicates or triplicates, except for ^{34}S, which was estimated from a set of

standards. Samples were prepared at the laboratory of the Mineralogia Aplicada i Geoquimica de Fluids research group (Universitat de Barcelona), whereas isotope analyses were performed at the Centres Científics i Tecnològics of Universitat de Barcelona.

3.4. Contribution of potential N sources

Following previous studies (e.g. Soto et al., 2019; Paredes et al., 2020), the relative contribution of potential N sources was estimated from $\delta^{15}N$ and $\delta^{18}O$ of NO_3^- using Bayesian mixing models (MixSIAR package in R; Moore and Semmens, 2008; Stock and Semmens 2016). The isotopic composition of the potential sources was assumed based on expected and measured δ-values from mineral fertilizers (NH_4^+ and NO_3^-), soil N, and manure and sewage (Vitòria et al., 2004; Kendall et al., 2008; Aravena and Mayer, 2009; Puig et al., 2016). The $\delta^{18}O_{NO3}$ values derived from the different N sources were calculated following Mayer et al. (2001). For that purpose, the following values were used: −6.4‰ and +0.0‰, for $\delta^{18}O_{H2O}$; +23.5‰ (Horibe et al., 1973), for atmospheric $\delta^{18}O_{O2}$. Atmospheric deposition of NO_3^- was not included as a source as measured $\delta^{18}O_{NO3}$ were far from those typical from atmospheric sources (>+50‰; Kendall et al., 2008). The following isotope values were used: i) NO_3^- fertilizers, +2 ± 8.5‰ and +21 ± 5.7‰, for $\delta^{15}N$ and $\delta^{18}O$, respectively; ii) NH_4^+ fertilizers, +2 ± 8.5‰ and +5.7 ± 3.0‰, for $\delta^{15}N$ and $\delta^{18}O$, respectively; iii) Soil N, +5.5 ± 3.5‰ and +5.7 ± 3.0‰, for $\delta^{15}N$ and $\delta^{18}O$, respectively; iv) Sewage and manure, +14 ± 8.5‰ and +5.7 ± 3.0‰, for $\delta^{15}N$ and $\delta^{18}O$, respectively. Into the mixing models, study area (Jarales and Brujuelo) and hydrogeological functioning of each site (Recharge/transition and discharge) were used as fixed effects. In addition, fractionation due to denitrification was not considered into the model. The models were run with three chains of 300,000 iterations, a burn-in of 200,000 and a thinning of 100.

4. Results

4.1. Hydrochemical data

Hydrochemical data for analyzed samples are presented in Table 2. Samples from Jarales and Brujuelo areas show a variable degree of mineralization, with a general trend to increase of EC values from the highest to the lowest altitudes (Table 1, Fig. 1). In Jarales area, the lowest EC value was found in Amarga wetland (JW2; 3.5 mS/cm), and the highest in Lower Anzur spring (JS2; 176 mS/cm). Similar drift was found in Brujuelo area: the lowest EC value was found in Cirueña wetland well (BP1; 4.2 mS/cm) and the highest in San Carlos spring (BS3; 196 mS/cm). Eh and DOC values follow the opposite altitudinal gradient: the highest values are associated to wetlands (JW1 and BW1), whereas the lowest values are found in brine springs (JS2, BS2, and BS3) (Table 2).

About N-species, NO_2^- and NO_3^- concentrations were below the LOD (0.005 mg/L) in 4 and 3 samples, respectively. The highest values for both compounds were found in Jarales well points: JP4 for NO_2^- (1.4 mg/L) and JP3 for NO_3^- (230 mg/L). These values do not seem to be influenced by mineralization, as observed for the rest of major ions (Table 2). NH_4^+ concentrations show a certain trend to higher values at the discharge points (JS2 and BS3).

Na–Cl and Ca–SO_4^{2-} are the principal hydrochemical facies in most of the water samples from both study areas (Fig. 2), with the exception of JP1 samples which shows a Mg–SO_4 composition. The high abundance of Cl^- (up to 94 and 128 g/L, in Jarales and Brujuelo springs, respectively) and Na^+ (up to 60 and 87 g/L, in Jarales and Brujuelo springs, respectively) defines the hypersaline nature of the water drained by the outlets. The rest of major ions, whose origin may be somewhat associated to evaporitic sources and possibly to carbonates rocks too, have lower concentrations (Table 2).

Samples with the highest EC values show molar Na^+/Cl^- ratios close to 1 (Table 2), typical from halite dissolution processes (e.g. Keuper evaporites). The lowest molar Na^+/Cl^- ratios are found in surface water control points, where meteoric water may have higher influence and wetlands sediments may favor ion exchange processes, as observed in previous works (Gil-Márquez, 2018). Values of molar Cl^-/Br^- ratio are shown in Fig. 3. They ranged from 400 (JW2 control point) to 6000 (BS2 control point). Jarales wetlands (JW1, JW2) present Cl^-/Br^- ratios close to rainwater (Cartwright et al., 2006).

In addition, the comparison of SO_4^{2-} and evaporite/carbonate-derived solutes is also shown in Table 2. With the exception of JP3 and JP4 samples, there is a slight enrichment of SO_4^{2-} compared to Ca^{2+}. As shown in previous studies (Gil-Márquez et al., 2017a), molar Ca^{2+}/Mg^{2+} ratios allow to distinguish two main groups. According to the 1:1 and 3:1

Table 2
Results of the chemical analyses in water samples (major ions in mg/L). Eh: redox potential (mV). DO: dissolved oxygen (mg/L). EC: electric conductivity (mS/cm). T: temperature (°C). DOC: dissolved organic carbon (mg/L). Alkalinity as (HCO_3^- + CO_3^{2-}). BLD: below limit of detection (<0.005 mg/L for NO_3^- and NO_2^-).

Control Point	JW1	JW2	JP1	JP2	JP3	JP4	JS1	JS2	BW1	BP1	BS1	BS2	BS3
Zone	Jarales wetland	Jarales wetland	Jarales well	Jarales well	Jarales well	Jarales well	Jarales spring	Jarales spring	Brujuelo wetland	Brujuelo well	Brujuelo spring	Brujuelo spring	Brujuelo spring
pH	9.3	8.6	7.6	7.8	7.5	7.2	7.0	7.1	8.3	7.7	7.7	7.0	6.4
Eh	+159	+72	+149	+150	+154	+189	+190	+18	+182	+168	+203	+194	+83
DO	7.56	11.1	1.46	1.04	0.88	0.44	1.54	3.42	6.22	6.54	5.52	3.01	1.74
EC	5.53	3.46	7.66	14.5	10.6	16.5	42.5	176	13.4	4.21	13.9	123	196
T	26.1	24.5	17.4	19.0	18.2	17.4	20.6	21.0	22.6	17.4	15.5	19.2	22.0
DOC	21.6	11.2	5.97	5.75	2.75	4.88	4.46	2.45	16.2	8.64	7.16	2.30	2.70
Cl	1227	732	789	5034	3001	5893	17,885	94,381	3968	502	4014	59,856	128,076
SO_4	2055	1180	4614	1456	1525	1009	4227	6205	2996	1474	3467	5837	6115
Alkalinity	54	110	639	730	313	234	355	254	75	395	190	186	216
Br	6.79	4.11	2.77	4.82	3.98	24.1	12.2	51.0	4.15	1.70	3.19	22.3	48.5
NO_2	BLD	BLD	0.449	BLD	0.746	1.40	0.348	0.164	BLD	0.027	0.045	0.076	0.013
NO_3	0.134	BLD	24.9	11.2	230	120	14.2	2.35	BLD	35.2	86.8	3.17	BLD
K	21	14	18	15	8	11	49	255	27	3	26	137	413
Ca	738	385	592	396	715	1542	1400	2243	574	446	775	2025	2402
Mg	188	170	977	231	290	803	317	430	601	256	426	391	582
Na	571	312	456	3336	1472	1027	11,543	60,184	2456	273	2304	41,675	86,976
NH_4	0.121	0.088	0.149	6.17	0.141	0.286	0.205	1.34	0.090	0.077	0.093	0.240	1.81
Na^+/Cl^-	0.72	0.66	0.89	1.02	0.76	0.27	1.00	0.99	0.96	0.84	0.89	1.08	1.05
SO_4^{2-}/Ca^{2+}	1.16	1.28	3.25	1.53	0.89	0.27	1.26	1.16	2.18	1.38	1.87	1.20	1.06
Ca^{2+}/Mg^{2+}	2.39	1.37	0.37	1.04	1.49	1.16	2.68	3.17	0.58	1.06	1.10	3.14	2.50

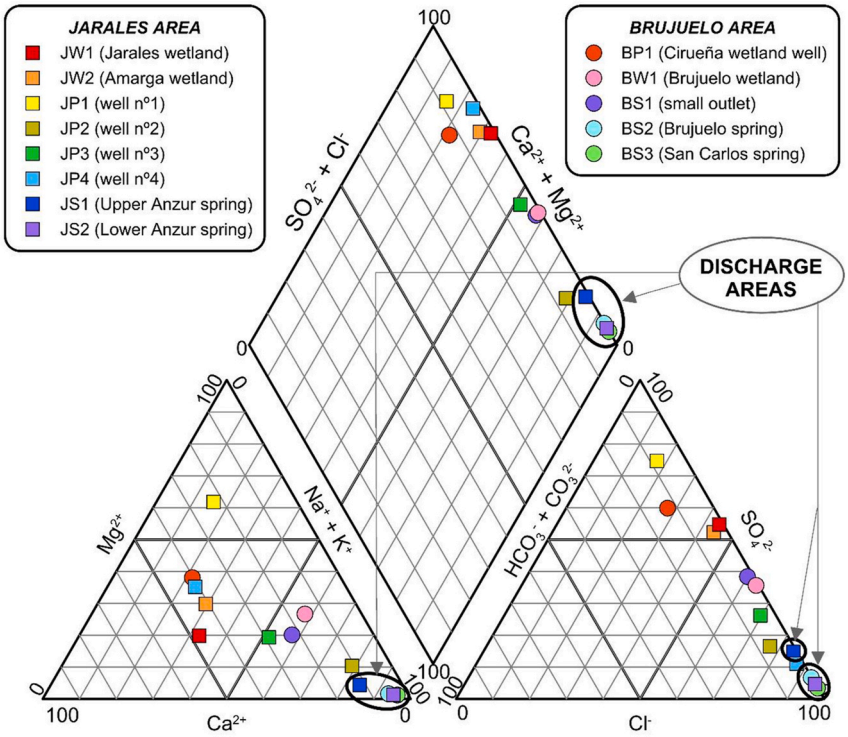

Fig. 2. Piper diagram showing the chemical composition of the water samples of the study.

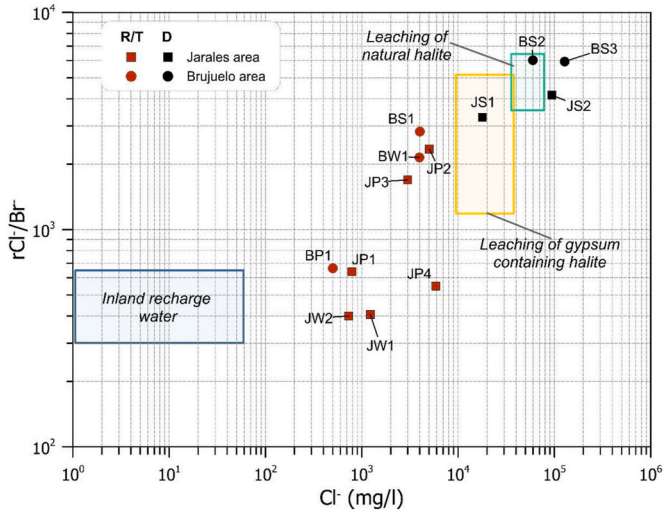

Fig. 3. Cl^- concentration versus molar Cl^-/Br^- ratio. R/T: Recharge/Transition; D: Discharge. Boxes including values of inland recharge water and leaching of natural halite and gypsum containing halite are obtained from Alcalá and Custodio (2008).

stoichiometric lines, when the values of Ca^{2+}/Mg^{2+} are close to 1 they indicate to dolomite dissolution, while they are related to dedolomitization processes or the mixture of limestone and dolomite present in the karst aquifer if they are near 3. Thus, Jarales wetlands (JW1 and JW2) and Brujuelo brine springs (BS2 and BS3) show a significant enrichment in Ca^{2+} compared to Mg^{2+}.

4.2. Isotope data in water samples

Complete isotope data in water samples are shown in Table 3. In Jarales, the average value of δ^2H_{H2O} in wetlands was +13.0 ± 5.2‰, whereas the $\delta^{18}O_{H2O}$ was +5.0 ± 1.6‰ in such sites. These values were considerable higher than those measured in wells (−33.4 ± 1.4‰ and −5.0 ± 0.2‰, for δ^2H_{H2O} and $\delta^{18}O_{H2O}$, respectively) and springs (−37.7 ± 0.8‰ and −5.7 ± 0.2‰, for δ^2H_{H2O} and $\delta^{18}O_{H2O}$, respectively). Concerning Brujuelo area, δ^2H_{H2O} and $\delta^{18}O_{H2O}$ showed values ranging from −42.4‰ and −5.7‰, respectively, in wetland samples (BW1), to −12.3‰ and 0‰, respectively, in well samples (BP1). The weighted average of $\delta^{18}O$ in the precipitation (−5.5‰) of the study area, from October 2014 to February 2017 (Gil-Márquez, 2018), was similar to those average values obtained in wells and springs from both Jarales and Brujuelo. In Fig. 4, samples from Jarales and Brujuelo areas are compared with the Global Meteoric Water Line (Craig, 1961), the Western Mediterranean Meteoric Water Line (Gat and Carmi, 1970), and the Local Meteoric Water Line.

In Jarales, the $\delta^{34}S_{SO4}$ showed an average value of +12.6 ± 7.7‰, with no big differences among wetlands (+13.5 ± 18.7‰), wells (+12.1 ± 4.4‰), and springs (+13.0 ± 0.1‰). Concerning $\delta^{18}O_{SO4}$, mean value in wetlands was +21.4 ± 4.9‰, slightly higher than those for wells (+13.1 ± 1.6‰) and springs (+12.5 ± 1.3‰). For Brujuelo samples, the $\delta^{34}S_{SO4}$ and $\delta^{18}O_{SO4}$ mean values were +12.9 ± 0.5‰ and +12.5 ± 1.1‰, respectively, with no big differences among habitats (Table 3). Such values of $\delta^{34}S_{SO4}$ and $\delta^{18}O_{SO4}$ in water samples are presented in Fig. 5 together with the range of potential SO_4^{2-} sources. Samples fall mainly within the range of evaporite minerals (gypsum) as natural source of sulfate, with a range of $\delta^{34}S_{SO4}$ between +12.5‰ and +16.6‰, and $\delta^{18}O_{SO4}$ between +8.9‰ and +16.9‰ (Ortí et al., 2014). However, some samples (JP3 and JP4) fall within anthropogenic sulfate range (fertilizers), with mean values of $\delta^{34}S_{SO4}$ around +5‰ and $\delta^{18}O_{SO4}$ around +12‰; Vitòria et al. (2004).

Due to the low NO_3^- concentration measured in some samples, $\delta^{15}N_{NO3}$ and $\delta^{18}O_{NO3}$ were only determined in eight of the thirteen samples. Isotope data are showed in Fig. 6, together with the range of potential NO_3^- sources (adapted from Puig et al. (2016) and references therein). $\delta^{18}O_{NO3}$ values deriving from nitrification of ammonium fertilizers and sewage/manure were calculated according to Mayer et al. (2001), applying values of −6.4‰ and +0.0‰ for $\delta^{18}O_{H2O}$, and +23.5‰

Table 3
Isotopic values (‰) in water samples: $\delta^{13}C$ in bicarbonate molecule, $\delta^{15}N$ and $\delta^{18}O$ in nitrate molecule, $\delta^{2}H$ and $\delta^{18}O$ in water molecule, $\delta^{34}S$ and $\delta^{18}O$ in sulfate molecule. nd: not determined.

	Control Point	Description	$\delta^{2}H_{H2O}$	$\delta^{18}O_{H2O}$	$\delta^{15}N_{NO3}$	$\delta^{18}O_{NO3}$	$\delta^{13}C_{DIC}$	$\delta^{34}S_{SO4}$	$\delta^{18}O_{SO4}$
Jarales	JW1	Wetland	+9.3	+3.8	nd	nd	nd	+0.2	+17.9
	JW2	Wetland	+16.6	+6.1	nd	nd	−10.0	+26.7	+24.9
	JP1	Well	−31.5	−4.9	+12.8	+9.1	−17.1	+13.4	+12.9
	JP2	Well	−33.3	−4.8	+8.6	+7.3	−20.1	+17.0	+15.3
	JP3	Well	−34.8	−5.2	+17.7	+14.2	−12.6	+11.4	+12.1
	JP4	Well	−34.0	−5.1	+16.0	+10.9	−15.7	+6.4	+11.9
	JS1	Spring	−37.1	−5.5	+13.7	+10.4	−10.7	+13.0	+13.4
	JS2	Spring	−38.2	−5.8	nd	nd	−11.1	+12.9	+11.6
	Wetland	Mean	+13.0	+5.0	nd	nd	−10.0	+13.5	+21.4
		SD	+5.2	+1.6	nd	nd	nd	+18.7	+4.9
	Well	Mean	−33.4	−5.0	+13.8	+10.4	−16.4	+12.1	+13.1
		SD	+1.4	+0.2	+4.0	+2.9	+3.1	+4.4	+1.6
	Spring	Mean	−37.7	−5.7	+13.7	+10.4	−10.9	+13.0	+12.5
		SD	+0.8	+0.2	nd	nd	+0.3	+0.1	+1.3
Brujuelo	BW1	Wetland	−42.4	−5.7	nd	nd	−14.1	+13.0	+12.4
	BP1	Well	−12.3	0.0	+13.7	+13.3	−19.5	+13.3	+14.2
	BS1	Spring	−28.6	−3.3	+3.5	+4.5	−13.2	+13.2	+12.9
	BS2	Spring	−39.2	−5.4	+16.3	+12.0	−6.7	+12.6	+11.5
	BS3	Spring	−40.8	−6.4	nd	nd	−6.9	+12.2	+11.7
	Spring	Mean	−36.2	−5.0	+9.9	+8.3	−8.9	+12.7	+12.0
		SD	+6.6	+1.6	+9.1	+5.3	+3.7	+0.5	+0.8

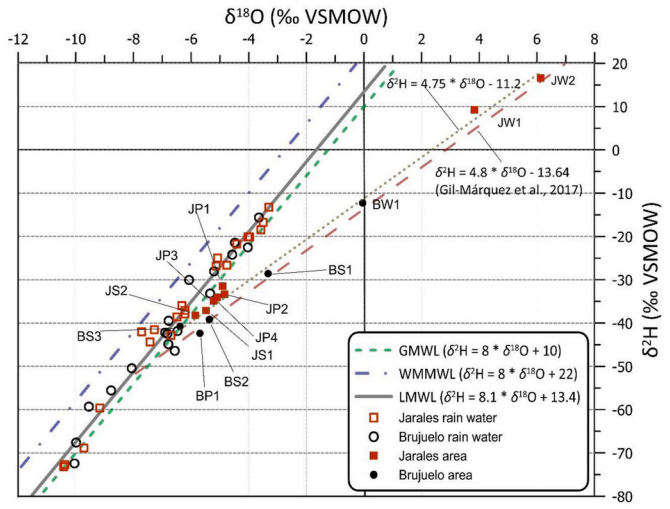

Fig. 4. $\delta^{18}O$ versus $\delta^{2}H$ plot including water samples from both study areas, Jarales rain, and Brujuelo rain (Gil-Márquez, 2018). R/T: Recharge/Transition; D: Discharge. Regression line ($\delta^{2}H = 4.75*\delta^{18}O - 11.2$) was calculated for all samples (n = 13) and compared with regression line calculated for wetland samples collected between September 2013 and June 2016 in Brujuelo area (Gil-Márquez et al., 2017a; $\delta^{2}H = 4.8*\delta^{18}O - 13.6$). Regression lines GMMW, WMMWL, and LMWL represent, respectively: The Global Meteoric Water Line (Craig, 1961), the Western Mediterranean Meteoric Water Line (Gat and Carmi, 1970), and the Local Meteoric Water Line from rainwater samples of the area.

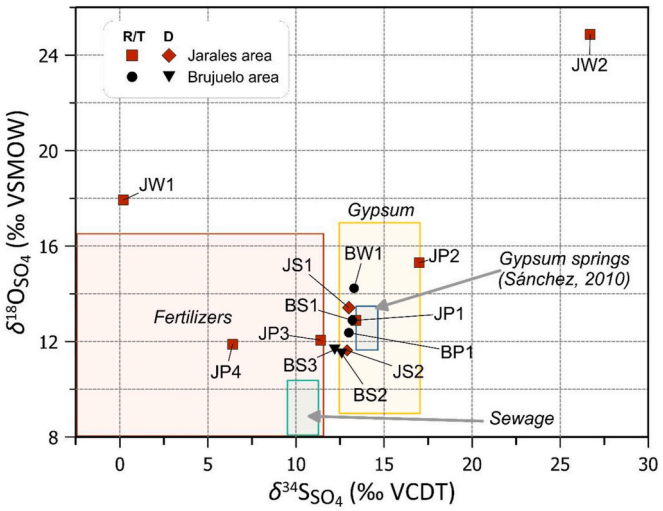

Fig. 5. $\delta^{34}S$ and $\delta^{18}O$ of dissolved SO_4^{2-} in the collected water samples from Jarales and Brujuelo area. R/T: Recharge/Transition; D: Discharge. The isotopic composition of the main sulfate sources is represented, including fertilizers (Vitòria et al., 2004), sewage (Otero et al., 2008), gypsum (Ortí et al., 2014), and gypsum springs in the CSC (Sánchez, 2010).

(Horibe et al., 1973) for atmospheric $\delta^{18}O_{O2}$. With the exception of JP2 and BS1 samples, all the samples fall over the range for soil N and manure nitrification.

Bayesian isotope mixing models suggested the contribution of each source to the NO_3^- load in Jarales and Brujuelo areas (Table 4). There were no significant differences ($p < 0.05$) between areas (Jarales and Brujuelo) or between sites with different hydrogeological functioning (recharge/transition and discharge). In all of them, NO_3^- fertilizers showed the highest contribution to total N with mean propotional contribution above 40% in all the locations. In contrast, soil N and NH_4^+ fertilizers had a lower estimated contribution: 12–14% and 10–13%, respectively.

In Jarales area, $\delta^{13}C_{DIC}$ average value was −13.9 ± 3.8‰, with well samples showing the lowest mean value (−16.4 ± 3.1‰) and similar mean values in wetlands (−10.0‰) and springs (−10.9 ± 0.3‰). The average values of $\delta^{13}C_{DIC}$ in Brujuelo were lower in wetlands (−14.1‰) and wells (−19.5‰) than in spring samples (−8.9 ± 3.7‰) (Table 3). These results show that most of the $\delta^{13}C_{DIC}$ values fall within the range of groundwater ($\delta^{13}C_{DIC}$ between −11‰ and −15‰; Vogel and Ehhalt, 1963) (Fig. 7). Jarales samples can be split into two groups: (1) wells and (2) spring and wetland waters. Well samples (JP1, JP2, and JP4) show $\delta^{13}C_{DIC}$ values between fertilizers (−30‰ and −24‰; from Vitòria et al., 2004), and typical groundwater, which helps to confirm nitrogen turnover assumptions in such control points. Spring and wetland waters (JW2, JS1, and JS2) drop between typical groundwater and atmospheric CO_2 (−8‰) given by Clark and Fritz (1997).

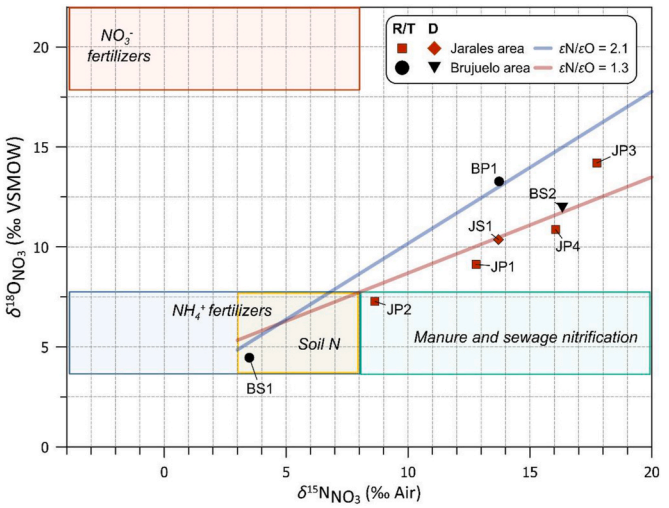

Fig. 6. $\delta^{15}N$ and $\delta^{18}O$ of dissolved NO_3^- in the collected water samples from Jarales and Brujuelo areas (n = 8). R/T: Recharge/Transition; D: Discharge. The isotopic composition of the main NO_3^- sources is represented: ammonium fertilizers, nitrate fertilizers, soil N, and manure and sewage nitrification (Vitòria et al., 2004; Kendall et al., 2008; Aravena and Mayer, 2009; Puig et al., 2016). Solid lines represent ε_N:ε_O determined in natural denitrification experiments: in red 1.3 from Fukada et al. (2003), and in blue 2.1 from Böttcher et al. (1990). (For interpretation of the references to color in this figure legend, the reader is referred to the Web version of this article.)

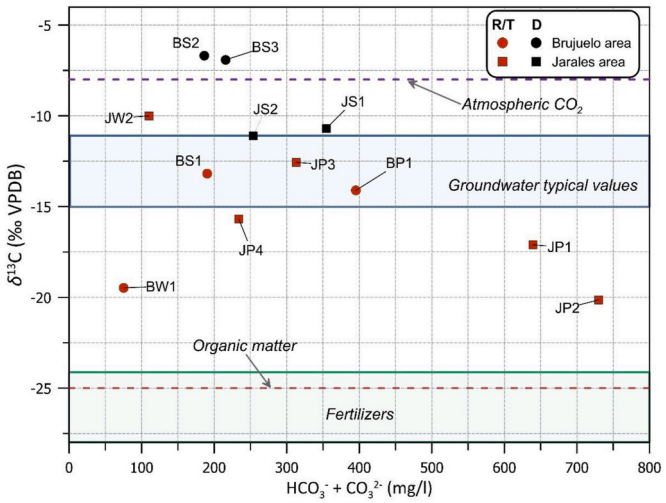

Fig. 7. Alkalinity ($HCO_3^- + CO_3^{2-}$) and $\delta^{13}C_{DIC}$ analyzed in water samples from Jarales and Brujuelo areas. R/T: Recharge/Transition; D: Discharge. The isotopic compositions of atmospheric CO_2, groundwater, organic matter, and fertilizers are represented (Vogel and Ehhalt, 1963; Clark and Fritz, 1997; Hoefs, 1997; Vitòria et al., 2004).

Table 4
Relative estimated contribution (%) of N sources to NO_3^- in the study areas. Estimation was made by using a two-isotope ($\delta^{15}N$ and $\delta^{18}O$ of dissolved NO_3^-) Bayesian mixing model which included area and hydrogeological functioning of each location as fixed effects. Fractionation due to denitrification was not considered into the model. Mean and SD of the Bayesian distribution are shown.

Area	Type	NH_4^+ fertilizers	NO_3^- fertilizers	Sewage/ manure	Soil N
Jarales	Recharge/ transition	13 ± 12	44 ± 18	29 ± 20	14 ± 13
	Discharge	11 ± 14	47 ± 25	29 ± 25	13 ± 15
Brujuelo	Recharge/ transition	12 ± 14	46 ± 24	29 ± 24	14 ± 16
	Discharge	10 ± 15	49 ± 28	29 ± 27	12 ± 16

5. Discussion

5.1. Groundwater recharge from wetlands areas

The first goal of this study was to determine the groundwater functioning in the two areas from the CSC: Jarales and Brujuelo. The results of this study confirm the existence of a hydrochemical gradient from recharge and transitional areas (wetlands and wells) to discharge areas (springs), supporting the findings from previous studies (Gil-Márquez, 2018). Groundwater functioning is illustrated in the conceptual model from Fig. 8. As shown in the results section, a progressive change of hydrochemical facies can be inferred from the hydrochemical alignment along calcium-magnesium and sulfate axis (Fig. 2). In addition, hydrochemical results suggest that regional groundwater is also able to interact with evaporitic deposits during its flow path towards discharge areas. As a result, solute contents increase in those areas (JS1, JS2, BS2, and BS3), reaching high salinity values (Table 2). Thus, these samples show the highest Cl^-/Br^- ratios (Fig. 3), falling close to the range of leaching of natural halite (Alcalá and Custodio, 2008). On the other hand, the low Cl^-/Br^- ratios and high SO_4^{2-} concentrations found in certain samples (JW1, JW2, JP1, and BP1) suggest that groundwater flowed through zones where halite was less abundant or absent. According to these Cl^-/Br^- ratios, geochemical evolution of groundwater is evident from recharge to discharge areas. Thus, groundwater interacts with minerals (i.e. gypsum and halite) present along the flow-path, leading to salinization (Belkhiri et al., 2012). However, the existence of mixing processes between recharge water and saline long-residence groundwater cannot be discarded.

Mineral leaching is also observed from chemical data (Table 2). Molar SO_4^{2-}/Ca^{2+} ratios close to 1 (e.g. JW1, JS2) are typical of gypsum dissolution processes from Keuper materials. Despite our results suggest dissolution, they must be taken with some caution due to calcite precipitation derived from the common ion effect (Appelo and Postma, 2005). Molar Ca^{2+}/Mg^{2+} ratios close to 1 (e.g. BP1, BS1, JP2) indicate dolomite dissolution, whereas ratio values around 3 (e.g. BS2, BS3, JS2) may be an indication of the presence of dedolomitization processes and/or the mixture of limestone and dolomite in the karst aquifer (DeGroot, 1967). The increase in Ca^{2+} availability due to gypsum dissolution promote calcite precipitation, decreasing its saturation state and enhancing dolomite dissolution (Wigley, 1973). Thus, groundwater dissolves evaporitic deposits of Keuper age, increasing salinity by the dissolution of minerals such as gypsum or halite. Our results verify the model presented by Andreo et al. (2016), confirming the hypothesis that wetlands and springs located in lower altitudinal zones act as discharge points for brine groundwater.

Concerning δ^2H_{H2O} and $\delta^{18}O_{H2O}$ data, the influence of precipitation and evaporation processes is clearly observed (Fig. 4). Evaporation processes are inferred from the slope of the regression line (4.75), which is similar to that obtained in Brujuelo area in the previous campaigns (4.80; Gil-Márquez et al., 2017a). Evaporation of rainwater causes a decrease in the slope of the $\delta^{18}O$ and δ^2H plots, from 8 towards ~3 due to equilibrium isotope fractionation (Clark and Fritz, 1997). The highest δ^2H_{H2O} and $\delta^{18}O_{H2O}$ values (+13.0 ± 5.2‰ and +5.0 ± 1.6‰, respectively) belong to wetland water in Jarales area, where the influence of evaporation is clearly observed. Such evaporated waters have little influence on groundwater recharge (i.e. BS1), whereas the rest of samples analyzed showed δ^2H_{H2O} and $\delta^{18}O_{H2O}$ values close to rain water values (Fig. 4). Therefore, precipitation seems to play a major role in groundwater recharge, with minimal evaporation effects. The recharge of groundwater is performed in the whole catchment, by concentrated infiltration through karst features (Gil-Márquez et al., 2017b) and

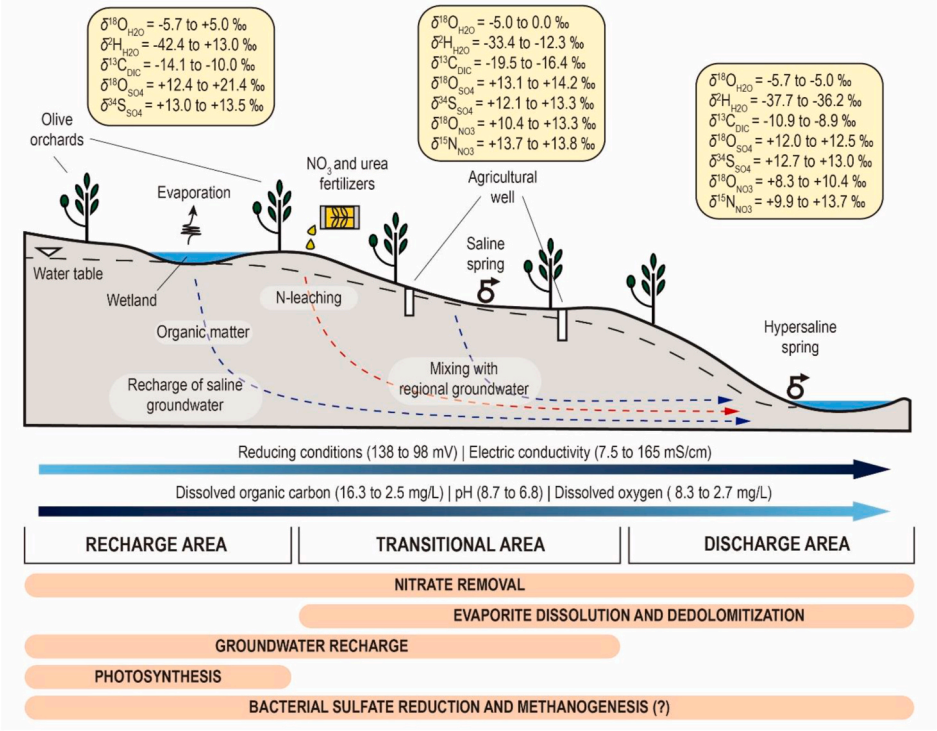

Fig. 8. Conceptual model for groundwater functioning in the CSC. Groundwater flows from recharge and transitional areas towards discharge areas show an evident evolution in physicochemical parameters and isotope compositions (mean values reported). The main hydrogeological and biogeochemical processes are noted in the model as discussed through the study.

probably by diffuse infiltration in permeable outcrops too.

5.2. Pollution removal in groundwater

While δ^2H_{H2O} and $\delta^{18}O_{H2O}$ provides valuable information on the hydrogeological functioning of the system, the inclusion of additional stable isotopes (i.e. $\delta^{34}S$, $\delta^{15}N$, $\delta^{13}C$) in the approach allows to trace and elucidate the underlying mechanisms of pollutant transport and removal (Hosono et al., 2011; Puig et al., 2013; Valiente et al., 2017). The current study found high concentrations of NO_3^- linked to transitional zones (e.g. JP3, JP4, BP1, and BS1). As described in Material and methods section, the field survey was carried out in spring-time. At this time of the year, fertilizers are widely used mainly as mineral and urea N-fertilizers directly applied on the olive-tree feet. The results of the Bayesian mixing model pointed out NO_3^- fertilizers as the main source of N in the study areas, with similar contributions in recharge/transition zones (44 ± 18% and 46 ± 24% in Jarales and Brujuelo, respectively) than in discharge areas (47 ± 25% and 49 ± 29% in Jarales and Brujuelo, respectively). Sewage and manure was the second source in importance, with a mean value of 29% in the whole catchment (Table 4). This source can be related to the application of urea which is subsequently mineralized and nitrified, as seawage waters and neither manure or slurry are used in Jarales and Brujuelo. Due to the limited number of samples used for building the model, we must be cautious about interpretation, and especially when distinguishing between NH_4^+ fertilizers and soil N, as both overlap in the isotopic composition of the sources. However, these findings support the hypothesis that groundwater recharge takes place throughout the whole catchment, as similar contributions of the sources are found no matter what type of zones they are. Therefore, the increase in NO_3^- concentrations in wells compared to wetlands may be reflecting this widespread groundwater recharge.

The regional groundwater flow can be contaminated by NO_3^- in both wetlands and wells, and transported together with other solutes from evaporitic deposits dissolution towards transitional and discharge areas (Fig. 8). Despite its lower concentrations, NO_2^- values also present a similar trend to that observed for NO_3^-. While no correlation is observed between NH_4^+ and NO_3^- concentrations, the highest NH_4^+ concentration is observed in wells (JP2; 6.2 mg/L), with significant values in the springs (1.34 mg/L and 1.81 mg/L, in JS2 and BS3, respectively).

In general, the lowest N-inorganic concentrations are found in discharge brine springs (JS1 and JS2 in Jarales, BS2, and BS3 in Brujuelo). In addition, low Eh values are coupled to high NH_4^+ concentrations in the most saline springs which are located in the final discharge points of each area (JS2 and BS3). Chemical data suggest that NO_3^- is removed through the groundwater flow, but these evidences can evidence that not only by denitrification (producing N_2) but also by DNRA (producing NH_4^+). Our $\delta^{18}O_{NO3}$ values were higher than those calculated following Mayer et al. (2001), N and O composition in the nitrate molecule should be modified by biological processes (e.g. denitrification in deep aquifer zones and/or dissimilation in wetlands). In addition, the higher DO concentrations found in wetland sites compared to well sites could also favor the occurrence of NO_3^- removal reactions (Soares, 2000).

The natural attenuation of NO_3^- under anoxic conditions (i.e. denitrification, DNRA) can be accomplished by heterotrophic denitrification using DOC as electron donor. As shown in Table 2, DOC may derive from recharge areas (i.e. JW1, BW1), where higher concentrations were found. Thus, nitrate removal should be responsible for the decrease in NO_3^- from transitional zones (i.e. JP3) to discharge springs (i.e. JS2). Despite only five samples from Jarales area had a high enough NO_3^- concentration to be isotopically characterized, denitrification and/or DNRA processes can explain the observed values. JP2 sample shows the highest NH_4^+ concentration and falls within the sewage/manure range, probably due to the application of urea N-fertilizers during spring time. The rest of the samples show an increasing $\delta^{15}N_{NO3}$ and $\delta^{18}O_{NO3}$ trend typical of denitrification (Korom, 1992) (Fig. 6). Such samples are close to the natural denitrification line (ε_N:ε_O of 1.3) reported by Fukada et al. (2003), and therefore, denitrification should be the main NO_3^- removal

pathway. In Jarales area, samples collected in wells JP1, JP3 and JP4 show $\delta^{15}N_{NO3}$ values fall within sewage/manure range, whereas $\delta^{18}O_{NO3}$ values are considerably higher than that range. The possible interference of mixing between NO_3^- and NH_4^+ in the wells cannot be ruled out. Volatilization of N-fertilizers increases both $\delta^{15}N_{NO3}$ and $\delta^{18}O_{NO3}$, in line with observed data. Moreover, the usage of NO_3^- fertilizers may lead to NO_2^- re-oxidation processes (Wunderlich et al., 2013). These processes occur during denitrification when NO_2^- is formed as an intermediate which can be quickly re-oxidized to NO_3^-. This reaction incorporates atoms of oxygen from ambient water, thus lowering $\delta^{18}O_{NO3}$. In conclusion, wells from Jarales are probably affected by denitrification and mixing of both (nitrate and urea) fertilizers, which is in line with the Bayesian model predictions.

About Brujuelo samples, three of them were analyzed for $\delta^{15}N_{NO3}$ and $\delta^{18}O_{NO3}$. BS1 sample drops into the range of soil organic N (between +3‰ and +8‰; Kendall et al., 2008). However, the role of volatilization and nitrification of ammonium fertilizers cannot be discarded as they produce isotopic signatures similar to those of soil NO_3^- (Vitòria et al., 2005). Moreover, the high NO_3^- concentration found in BS1 sample (86.8 mg/L) is in line with this hypothesis. BP1 and BS2 show higher values of $\delta^{15}N_{NO3}$ vs $\delta^{18}O_{NO3}$ in Fig. 6, falling within the denitrification lines reported by Böttcher et al. (1990) and Fukada et al. (2003), respectively (Fig. 6). Thus, denitrification processes can be major contributors to NO_3^- attenuation in both control points, but DNRA cannot be discarded. Previous studies in karst systems also used $\delta^{15}N_{NO3}$ and $\delta^{18}O_{NO3}$ vs Ln(NO_3^-) ratios to explain the sources and fate of nitrate (Yue et al., 2015). However, due to the limited number of data available, the evidence obtained by this means does not provide more information than that stated above. In surface wetland waters (i.e. JW2, and BW1), the low NO_3^- levels found (below the LOD) can be indicative of dissimilation processes linked to the sediment-water interface, including denitrification or DNRA.

NO_3^- is commonly used in uncontaminated karst aquifers as infiltration tracers to assess the water flow coming or the unsaturated zone (Mahler and Garner, 2009; Mudarra and Andreo, 2011). Fertilizing practices and sewage, as stated in the present study, can result in rising the concentration NO_3^- in the groundwater of karst systems (Peterson et al., 2002; Lorette et al., 2020). Recent research has showed that denitrification can occur in both oxic and anoxic areas of karst freshwater aquifers (Henson et al., 2017), mainly related to soil and epikarst environments (Husic et al., 2019; Ming et al., 2020). In that sense, the results obtained in the present work are novel as NO_3^- removal within the karst strongly depends on the long residence time of the CSC.

High DOC values measured in such samples can promote heterotrophic denitrification, but also other redox reactions like bacterial sulfate reduction (BSR) and methanogenesis. There reactions require organic matter as electron donor, which may be autochthonous (e.g. from primary producers) and allochthonous (e.g. from sewage). In the study areas, it may be produced by autotrophs in surface waters of transitional areas, and then transported to deeper zones of the aquifer by regional groundwater flows. Isotope values ($\delta^{13}C_{DIC}$) are among the typical DIC biogenic (−26 to −18‰), geogenic (−12‰–5‰) and atmospheric sources (−15% to 8‰) (Campeau et al., 2017; and references therein). Among the processes that can modify the isotopic composition of $\delta^{13}C_{DIC}$ are: i) photosynthesis; ii) methanogenesis; iii) DOC mineralization; iv) CH_4 oxidation. The first two lead to $\delta^{13}C_{DIC}$ increase with a slightly decrease in DIC concentration. Assuming that organic matter is mainly autochthonous in the study areas, this trend is observed from recharge/transition (JP1 and JP2, Fig. 7) to discharge areas (BS2 and BS3). This is also evidenced in BW1 sample, a wetland site where primary producers must be very active resulting in an isotopic discrimination of carbon during photosynthesis (Boutton, 1991). In addition, gas bubbling was observed during sample collection in both sites, which can indicate bacterial-mediated redox reactions like bacterial sulfate reduction (BSR) and methanogenesis able to increase $\delta^{13}C_{DIC.}$ DOC mineralization and CH_4 oxidation have an opposite effect: increase DIC coupled to $\delta^{13}C_{DIC}$ decrease. Although the existence of these processes cannot be ruled out, these trends are not observed in our samples. Therefore, $\delta^{13}C_{DIC}$ values are in accordance with previous discussion about solute transport from wetlands and wells to springs.

As stated above, BSR can modify the isotopic composition of both DIC and dissolved SO_4^{2-}, hampering the interpretation of hydrogeological processes. The necessary conditions for BSR processes, DOC availability and anaerobic conditions (Nordstrom et al., 2007), are found in the study areas (Table 2). During BSR, bacteria preferably consume ^{32}S compared to ^{34}S, increasing $\delta^{34}S$ values in residual SO_4^{2-} (Strebel et al., 1990). According to that, BSR processes could only be clearly suggested in JW2 sample (Fig. 5). Despite BSR cannot be confirmed neither discarded in the remaining samples, observed $\delta^{34}S_{SO4}$ and $\delta^{18}O_{SO4}$ values can be explained by mixing and dissolution processes. Such values are close to gypsum isotope composition in most of the samples (Sánchez, 2010). Therefore, water from recharge would be able to dissolve gypsum deposits, explaining the increase in both salt concentrations (Table 2), as well as $\delta^{34}S_{SO4}$ and $\delta^{18}O_{SO4}$ values (Table 3). These findings support the purposed conceptual model of the system, and improve our understanding of the complex groundwater functioning of evaporitic karst systems.

6. Conclusions

The purpose of the current study was to understand the pollutant removal within the Chaotic Subbetic Complexes and to validate its hydrogeological functioning model by combining geochemical and isotopic data. The results confirm the complex hydrochemical and biogeochemical processes that occur in this singular evaporitic karst system. Hydrochemical data suggest the existence of regional flows from recharge areas, less mineralized, to the discharge zone, showing the highest salinities. Along the way, groundwater dissolves evaporitic deposits of Keuper age, increasing salinity by the dissolution of minerals such as gypsum or halite. Isotope data also confirm this connection between mineralized groundwater in deep parts of the aquifer and surface water of wetlands. Precipitation, and to a lesser extent evaporation, are the main drivers of groundwater recharge in the whole catchment.

In these evaporitic kars systems, long-residence groundwater also plays an important role in the biogeochemical evolution. Bayesian mixing models show that the origin of NO_3^- in the study areas is mainly related to nitrate and urea fertilizers. Nitrate removal processes are found in transitional zones and discharge springs linked to the highest salinity values. Denitrification in Jarales and Brujuelo seems to be the main removal pathway, but DNRA cannot be discarded. Both processes are linked to organic carbon oxidation, which is produced by autotrophs in recharge areas (wetlands) and then transported to deeper zones of the aquifer by regional groundwater flow. The origin of sulfate in the study areas is predominatly linked to evaporite (gypsum) dissolution. While bacterial sulfate reduction processes cannot be ruled out, isotope data highlight the importance of mixing and gypsum dissolution processes.

This study provides the first comprehensive understanding of the nitrate fate in an evaporitic karst system where deep hypersaline groundwater plays a key role. The potential of these systems to remove pollutants must be taken into account in order to plan agricultural activities and protection strategies. Further field work is needed to fully understand the implications of biogeochemical recycling in such unique systems.

Declaration of competing interest

The authors declare that they have no known competing financial interests or personal relationships that could have appeared to influence the work reported in this paper.

Acknowledgements

The work was funded by the Excellence Projects P11-RNM-8087 and P10-RNM-6895R and the Research Group RNM-308 of the Autonomous Government of Andalusia (Spain), SBPLY/17/180501/000296 of the Castilla-La Mancha Government (Spain), and project CICYT-CGL2017-87216-C4-2-R from the Spanish Government. The authors wish to thank the Centres Científics i Tecnològics of Universitat de Barcelona the Servicios de Apoyo a la Investigación (SAI) of the University of A Coruña for isotope and chemical analyses.

References

Albertin, A.R., Sickman, J.O., Pinowska, A., Stevenson, R.J., 2012. Identification of nitrogen sources and transformations within karst springs using isotope tracers of nitrogen. Biogeochemistry 108 (1–3), 219–232.

Alcalá, F.J., Custodio, E., 2008. Using the Cl/Br ratio as a tracer to identify the origin of salinity in aquifers in Spain and Portugal. J. Hydrol. 359 (1–2), 189–207.

Andreo, B., Gil-Márquez, J.M., Mudarra, M., Linares, L., Carrasco, F., 2016. Hypothesis on the hydrogeological context of wetland areas and springs related to evaporitic karst aquifers (Málaga, Córdoba and Jaén provinces, Southern Spain). Environmental Earth Sciences 75 (9), 759.

APHA, AVWA, W., 2012. Standard Methods for Examination of Water and Wastewater, twenty-second ed. American Public Health Association, Washington, D.C.

Appelo, C.A.J., Postma, D., 2005. Geochemistry, Groundwater and Pollution, 2nd. Balkema, Rotterdam.

Aravena, R., Mayer, B., 2009. Isotopes and processes in the nitrogen and sulfur cycles. Environmental isotopes in biodegradation and bioremediation 203–246.

Ayadi, Y., Mokadem, N., Besser, H., Khelifi, F., Harabi, S., Hamad, A., Boyce, A., Laouar, R., Hamed, Y., 2018. Hydrochemistry and stable isotopes (δ18O and δ2H) tools applied to the study of karst aquifers in Southern Mediterranean basin (Teboursouk area, NW Tunisia). J. Afr. Earth Sci. 137, 208–217.

Baker, L.A., 1998. Design considerations and applications for wetland treatment of high-nitrate waters. Water Sci. Technol. 38 (1), 389–395.

Barbieri, M., Boschetti, T., Petitta, M., Tallini, M., 2005. Stable isotope (2H, 18O and 87Sr/86Sr) and hydrochemistry monitoring for groundwater hydrodynamics analysis in a karst aquifer (Gran Sasso, Central Italy). Appl. Geochem. 20 (11), 2063–2081.

Barnes, C.J., Allison, G.B., 1988. Tracing of water movement in the unsaturated zone using stable isotopes of hydrogen and oxygen. J. Hydrol. 100 (1–3), 143–176.

Belkhiri, L., Mouni, L., Tiri, A., 2012. Water–rock interaction and geochemistry of groundwater from the Ain Azel aquifer, Algeria. Environ. Geochem. Health 34 (1), 1–13.

Bhagowati, B., Ahamad, K.U., 2019. A review on lake eutrophication dynamics and recent developments in lake modeling. Ecohydrol. Hydrobiol. 19, 155–166. https://doi.org/10.1016/j.ecohyd.2018.03.002.

Böttcher, J., Strebel, O., Voerkelius, S., Schmidt, H.L., 1990. Using isotope fractionation of nitrate-nitrogen and nitrate-oxygen for evaluation of microbial denitrification in a sandy aquifer. J. Hydrol. 114 (3–4), 413–424.

Boutton, T.W., 1991. Stable Carbon Isotope Ratios of Natural Materials: II. Atmospheric, Terrestrial, Marine, and Freshwater Environments. In: Coleman, David C., Fry, Brian (Eds.), Carbon Isotope Techniques. Academic Press, pp. 173–185. ISBN 9780121797300. https://doi.org/10.1016/B978-0-12-179730-0.50016-3.

Boyd, C.E., 2020. Water Quality. An Introduction, 3rd. Ed. Springer Nature, Rotterdam.

Calaforra, J.M., Pulido-Bosch, A., 1999. Gypsum karst features as evidence of diapiric processes in the Betic Cordillera, Southern Spain. Geomorphology 29 (3–4), 251–264.

Campeau, A., Wallin, M.B., Giesler, R., Löfgren, S., Mörth, C.M., Schiff, S., Venkiteswaran, J.J., Bishop, K., 2017. Multiple sources and sinks of dissolved inorganic carbon across Swedish streams, refocusing the lens of stable C isotopes. Sci. Rep. 7 (1), 1–14.

Canfield, D.E., Glazer, A.N., Falkowski, P.G., 2010. The evolution and future of Earth's nitrogen cycle. Science 330 (6001), 192–196.

Carrasco, F., 1986. Contribucion al conocimiento de la cuenca alta del rio Guadalhorce: el medio físico. PhD Thesis Universidad de Granada. Hidrogeoquimica.

Cartwright, I., Weaver, T.R., Fifield, L.K., 2006. Cl/Br ratios and environmental isotopes as indicators of recharge variability and groundwater flow: an example from the southeast Murray Basin, Australia. Chem. Geol. 231 (1–2), 38–56.

Caschetto, M., Colombani, N., Mastrocicco, M., Petitta, M., Aravena, R., 2017. Nitrogen and sulphur cycling in the saline coastal aquifer of Ferrara, Italy. A multi-isotope approach. Appl. Geochem. 76, 88–98.

Clark, I., Fritz, P., 1997. The environmental isotopes. Environmental Isotopes in Hydrogeology 2–34.

Comly, H.H., 1945. Cyanosis in infants caused by nitrates in well water. J. Am. Med. Assoc. 129 (2), 112–116.

Craig, H., 1961. Isotopic variations in meteoric waters. Science 133 (3465), 1702–1703.

Dassenakis, M., Scoullos, M., Foufa, E., Krasakopoulou, E., Pavlidou, A., Kloukiniotou, M., 1998. Effects of multiple source pollution on a small Mediterranean river. Appl. Geochem. 13 (2), 197–211.

DeGroot, K., 1967. Experimental dedolomitization. J. Sediment. Res. 37 (4), 1216–1220.

Destouni, G., Darracq, A., 2009. Nutrient cycling and N_2O emissions in a changing climate: the subsurface water system role. Environ. Res. Lett. 4 https://doi.org/10.1088/1748-9326/4/3/035008.

Dodds, W.K., 2006. Eutrophication and trophic state in rivers and streams. Limnol. Oceanogr. 51, 671–680. https://doi.org/10.4319/lo.2006.51.1_part_2.0671.

Dogramaci, S.S., Herczeg, A.L., Schiff, S.L., Bone, Y., 2001. Controls on δ34S and δ18O of dissolved sulfate in aquifers of the Murray Basin, Australia and their use as indicators of flow processes. Appl. Geochem. 16 (4), 475–488.

EC, 1998. Council Directive 98/83/EC, of 3 November 1998, relative to human drinking water quality [online] Off J Eur Communities Law 330.

EC, 2006. Council Directive 2006/118/EC, of 12 December 2006, on the protection of groundwater against pollution and deterioration [online]. Off J Eur Union Law 372, 19–31.

Egbi, C.D., Anornu, G., Appiah-Adjei, E.K., Ganyaglo, S.Y., Dampare, S.B., 2018. Evaluation of water quality using hydrochemistry, stable isotopes, and water quality indices in the Lower Volta River Basin of Ghana. Environ. Dev. Sustain. 1–31.

Einsiedl, F., Maloszewski, P., Stichler, W., 2009. Multiple isotope approach to the determination of the natural attenuation potential of a high-alpine karst system. J. Hydrol. 365 (1–2), 113–121.

Epstein, S., Mayeda, T., 1953. Variation of O18 content of waters from natural sources. Geochem. Cosmochim. Acta 4 (5), 213–224.

Fisher, J., Acreman, M.C., 2004. Wetland nutrient removal: a review of the evidence. Hydrol. Earth Syst. Sci. Discuss. 8 (4), 673–685.

Fraser, P., Chilvers, C., 1981. Health aspects of nitrate in drinking water. Sci. Total Environ. 18, 103–116.

Fukada, T., Hiscock, K.M., Dennis, P.F., Grischek, T., 2003. A dual isotope approach to identify denitrification in groundwater at a river-bank infiltration site. Water Res. 37 (13), 3070–3078.

Gammons, C.H., Brown, A., Poulson, S.R., Henderson, T.H., 2013. Using stable isotopes (S, O) of sulfate to track local contamination of the Madison karst aquifer, Montana, from abandoned coal mine drainage. Appl. Geochem. 31, 228–238.

García-Robledo, E., Corzo, A., Papaspyrou, S., 2014. A fast and direct spectrophotometric method for the sequential determination of nitrate and nitrite at low concentrations in small volumes. Mar. Chem. 162, 30–36.

Gat, J.R., Carmi, I., 1970. Evolution of the isotopic composition of atmospheric waters in the Mediterranean Sea area. J. Geophys. Res. 75 (15), 3039–3048.

Gil-Márquez, J.M., 2018. Caracterización hidrogeológica de humedales y manantiales salinos asociados a acuíferos kársticos evaporíticos del sector central del subbético. PhD Thesis Universidad de Granada.

Gil-Márquez, J.M., Barberá, J.A., Andreo, B., Mudarra, M., 2017a. Hydrological and geochemical processes constraining groundwater salinity in wetland areas related to evaporitic (karst) systems. A case study from Southern Spain. J. Hydrol. 544, 538–554.

Gil-Márquez, J.M., Barberá, J.A., Mudarra, M., Andreo, B., Prieto-Mera, J., Sánchez, D., Rizo-Decelis, D., Argamasilla, M., Nieto, J.M., de la Torre, B., 2017b. Karst development of an evaporitic system and its hydrogeological implications inferred from GIS-based analysis and tracing techniques. Int. J. Speleol. 46 (2), 219.

Gil-Márquez, J.M., Sültenfuß, J., Andreo, B., Mudarra, M., 2020. Groundwater dating tools (^{3}H, ^{3}He, ^{4}He, CFC-12, SF_6) coupled with hydrochemistry to evaluate the hydrogeological functioning of complex evaporite-karst settings. J. Hydrol. 580, 124263. https://doi.org/10.1016/j.jhydrol.2019.124263.

Gilbert, J.D., Guerrero, F., de Vicente, I., 2014. Sediment desiccation as a driver of phosphate availability in the water column of Mediterranean wetlands. Sci. Total Environ. 466, 965–975.

Gómez-Alday, J.J., Carrey, R., Valiente, N., Otero, N., Soler, A., Ayora, C., Sanz, D., Muñoz-Martín, A., Castaño, S., Recio, C., Carnicero, A., Cortijo, A., 2014. Denitrification in a hypersaline lake–aquifer system (Pétrola Basin, Central Spain): the role of recent organic matter and Cretaceous organic rich sediments. Sci. Total Environ. 497, 594–606.

González-Ramón, A., López-Chicano, M., Gázquez, F., Durán-Valsero, J.J., Pedrera, A., Ruiz-Constán, A., González-Egea, E., 2017. Isotopic and hydrochemistry spatial variation of sulfate for groundwater characterization in karstic aquifers. Hydrol. Process. 31 (18), 3242–3254.

Gutiérrez, F., Calaforra, J.M., Cardona, F., Ortí, F., Durán, J.J., Garay, P., 2008. Geological and environmental implications of the evaporite karst in Spain. Environ. Geol. 53 (5), 951–965.

Hall, L.W., Anderson, R.D., 1995. The influence of salinity on the toxicity of various classes of chemicals to aquatic biota. Crit. Rev. Toxicol. 25 (4), 281–346.

Henson, W.R., Huang, L., Graham, W.D., Ogram, A., 2017. Nitrate reduction mechanisms and rates in an unconfined eogenetic karst aquifer in two sites with different redox potential. J. Geophys. Res.: Biogeosciences 122 (5), 1062–1077.

Hoefs, J., 2009. Stable Isotope Geochemistry, 285. springer, Berlin.

Hood-Nowotny, R., Umana, N.H.N., Inselbacher, E., Oswald-Lachouani, P., Wanek, W., 2010. Alternative methods for measuring inorganic, organic, and total dissolved nitrogen in soil. Soil Sci. Soc. Am. J. 74 (3), 1018–1027.

Horibe, Y., Shigehara, K., Takakuwa, Y., 1973. Isotope separation factor of carbon dioxide-water system and isotopic composition of atmospheric oxygen. J. Geophys. Res. 78 (15), 2625–2629.

Hosono, T., Wang, C.H., Umezawa, Y., Nakano, T., Onodera, S.I., Nagata, T., Yoshimizu, C., Tayasu, I., Taniguchi, M., 2011. Multiple isotope (H, O, N, S and Sr) approach elucidates complex pollution causes in the shallow groundwaters of the Taipei urban area. J. Hydrol. 397 (1–2), 23–36.

Hosono, T., Lorphensriand, O., Onodera, S.I., Okawa, H., Nakano, T., Yamanaka, T., Tsujimura, M., Taniguchi, M., 2014. Different isotopic evolutionary trends of δ34S and δ18O compositions of dissolved sulfate in an anaerobic deltaic aquifer system. Appl. Geochem. 46, 30–42.

Husic, A., Fox, J., Adams, E., Ford, W., Agouridis, C., Currens, J., Backus, J., 2019. Nitrate pathways, processes, and timing in an agricultural karst system: development and application of a numerical model. Water Resour. Res. 55 (3), 2079–2103.
Jambrina-Enríquez, M., Recio, C., Armenteros, I., 2018. Biogeochemical characterization of a Mediterranean shallow lake using stable isotopes: laguna del Cristo (NW Iberian Peninsula). Environmental earth sciences 77 (2), 49.
Katz, B.G., Chelette, A.R., Pratt, T.R., 2004. Use of chemical and isotopic tracers to assess nitrate contamination and ground-water age, Woodville Karst Plain, USA. J. Hydrol. 289 (1–4), 36–61.
Kendall, C., McDonnell, J.J., 2012. Isotope Tracers in Catchment Hydrology. Elsevier.
Kendall, C., Elliott, E.M., Wankel, S.D., 2008. Tracing anthropogenic inputs of nitrogen to ecosystems. Stable isotopes in ecology and environmental science 2, 375–449.
Korom, S.F., 1992. Natural denitrification in the saturated zone: a review. Water Resour. Res. 28 (6), 1657–1668.
Kraft, G.J., Stites, W., 2003. Nitrate impacts on groundwater from irrigated-vegetable systems in a humid north-central US sand plain. Agric. Ecosyst. Environ. 100 (1), 63–74.
Li, S.L., Liu, C.Q., Lang, Y.C., Tao, F., Zhao, Z., Zhou, Z., 2008. Stable carbon isotope biogeochemistry and anthropogenic impacts on karst ground water, Zunyi, Southwest China. Aquat. Geochem. 14 (3), 211.
Lorette, G., Peyraube, N., Lastennet, R., Denis, A., Sabidussi, J., Fournier, M., Viennet, D., Gonand, J., Villanueva, J.D., 2020. Tracing water perturbation using NO3−, doc, particles size determination, and bacteria: a method development for karst aquifer water quality hazard assessment. Sci. Total Environ. 725.
Lowe, E.F., Keenan, L.W., 1997. Managing phosphorus-based, cultural eutrophication in wetlands: a conceptual approach. Ecol. Eng. 9, 109–118. https://doi.org/10.1016/S0925-8574(97)00035-9.
Mahler, B.J., Garner, B.D., 2009. Using nitrate to quantify quick flow in a karst aquifer. Ground Water 47 (3), 350–360.
Margalef-Marti, R., Carrey, R., Viladés, M., Jubany, I., Vilanova, E., Grau, R., Soler, A., Otero, N., 2019. Use of nitrogen and oxygen isotopes of dissolved nitrate to trace field-scale induced denitrification efficiency throughout an in-situ groundwater remediation strategy. Sci. Total Environ. 686, 709–718.
Martín-Serrano, A., 1986. Mapa geológico de la Hoja no 1006 (Benamejí), *Mapa Geológico de España* E. 1:50 000. Segunda Serie (Magna).
Mas-Pla, J., Menció, A., 2019. Groundwater nitrate pollution and climate change: learnings from a water balance-based analysis of several aquifers in a western Mediterranean region (Catalonia). Environ. Sci. Pollut. Control Ser. 26 (3), 2184–2202.
Mayer, B., Bollwerk, S.M., Mansfeldt, T., Hütter, B., Veizer, J., 2001. The oxygen isotope composition of nitrate generated by nitrification in acid forest floors. Geochem. Cosmochim. Acta 65 (16), 2743–2756.
McIlvin, M.R., Altabet, M.A., 2005. Chemical conversion of nitrate and nitrite to nitrous oxide for nitrogen and oxygen isotopic analysis in freshwater and seawater. Anal. Chem. 77 (17), 5589–5595.
Mills, C.T., Goldhaber, M.B., Stricker, C.A., Holloway, J.M., Morrison, J.M., Ellefsen, K. J., Rosenberry, D.O., Thurston, R.S., 2011. Using stable isotopes to understand hydrochemical processes in and around a Prairie Pothole wetland in the Northern Great Plains, USA. Appl. Geochem. 26, S97–S100.
Ming, X., Groves, C., Wu, X., Chang, L., Zheng, Y., Yang, P., 2020. Nitrate migration and transformations in groundwater quantified by dual nitrate isotopes and hydrochemistry in a karst World Heritage site. Sci. Total Environ. 735.
Moore, J.W., Semmens, B.X., 2008. Incorporating uncertainty and prior information into stable isotope mixing models. Ecol. Lett. 11 (5), 470–480.
Mudarra, M., Andreo, B., 2011. Relative importance of the saturated and the unsaturated zones in the hydrogeological functioning of karst aquifers: the case of Alta Cadena (Southern Spain). J. Hydrol. 397 (3–4), 263–280.
Nichols, D.S., 1983. Capacity of natural wetlands to remove nutrients from wastewater. Journal (Water Pollution Control Federation) 495–505.
Nordstrom, D.K., Wright, W.G., Mast, M.A., Bove, D.J., Rye, R.O., 2007. Aqueous-sulfate stable isotopes—a study of mining-affected and undisturbed acidic drainage. U. S. Geol. Surv. Prof. Pap. 1651, 387–416.
Novales de, C., Recio, J.M., Medina, M., 1991. Evaluacion de los niveles de metales pesados en ecosistemas endorreicos. Ecología 5, 63–71.
Ortí, F., Pérez-López, A., García-Veigas, J., Rosell, L., Cendón, D.I., Pérez-Valera, F., 2014. Sulfate isotope compositions (34S, 18O) and strontium isotopic ratios (87sr/86sr) of triassic evaporites in the betic cordillera (SE Spain). Rev. Soc. Geol. Espana 27 (1), 79–89.
Otero, N., Soler, A., Canals, À., 2008. Controls of δ34S and δ18O in dissolved sulphate: learning from a detailed survey in the Llobregat River (Spain). Appl. Geochem. 23 (5), 1166–1185.
Panno, S.V., Hackley, K.C., Hwang, H.H., Kelly, W.R., 2001. Determination of the sources of nitrate contamination in karst springs using isotopic and chemical indicators. Chem. Geol. 179 (1–4), 113–128.
Paredes, I., Otero, N., Soler, A., Green, A.J., Soto, D.X., 2020. Agricultural and urban delivered nitrate pollution input to Mediterranean temporary freshwaters. Agric. Ecosyst. Environ. 294, 106859.
Peterson, E.W., Davis, R.K., Brahana, J.V., Orndorff, H.A., 2002. Movement of nitrate through regolith covered karst terrane, northwest Arkansas. J. Hydrol. 256 (1–2), 35–47.
Puig, R., Folch, A., Menció, A., Soler, A., Mas-Pla, J., 2013. Multi-isotopic study (15N, 34S, 18O, 13C) to identify processes affecting nitrate and sulfate in response to local and regional groundwater mixing in a large-scale flow system. Appl. Geochem. 32, 129–141.
Puig, R., Soler, A., Widory, D., Mas-Pla, J., Domènech, C., Otero, N., 2016. Characterizing sources and natural attenuation of nitrate contamination in the Baix Ter aquifer system (NE Spain) using a multi-isotope approach. Sci. Total Environ. 580, 518–532.
Rodríguez-Fernández, J., Roldán, F.J., Azañón, J.M., García-Cortés, A., 2013. El colapso gravitacional del frente orogénico alpino en el Dominio Subbético durante el Mioceno medio-superior: el Complejo Extensional Subbético. Bol. Geol. Min. 124, 477–504.
Rodríguez-Rodríguez, M., Moral, F., Benavente, J., 2009. Grado de dependencia de las aguas subterráneas, índice de funcionamiento hidrológico y principales amenazas en los principales humedales continentales de la depresión del Guadalquivir. Bol. Geol. Min. 120, 347–360.
Roldán, F.J., 1995. *Evolución Neógena de la Cuenca del Guadalquivir*. PhD Thesis. Univ. Granada.
Ryabenko, E., Altabet, M.A., Wallace, D.W., 2009. Effect of chloride on the chemical conversion of nitrate to nitrous oxide for δ15N analysis. Limnol Oceanogr. Methods 7 (7), 545–552.
Sánchez, D., 2010. Aplicación de la Directiva Marco del Agua 2000/60/CE en la cuenca hidrográfica del río Guadalhorce (Málaga). Caracterización inicial. PhD Thesis University of Málaga.
Santoro, A.E., 2010. Microbial nitrogen cycling at the saltwater–freshwater interface Alyson. Hydrogeol. J. 18, 187–202. https://doi.org/10.1007/s10040-009-0526-z.
Serrano, L., Reina, M., Quintana, X.D., Romo, S., Olmo, C., Soria, J.M., Blanco, S., Fernández-Aláez, C., Fernández-Aláez, M., Caria, M.C., Bagella, S., Kalettka, T., Pätzig, M., 2017. A new tool for the assessment of severe anthropogenic eutrophication in small shallow water bodies. Ecol. Indicat. 76, 324–334. https://doi.org/10.1016/j.ecolind.2017.01.034.
Smolders, A.J., Lucassen, E.C., Bobbink, R., Roelofs, J.G., Lamers, L.P., 2010. How nitrate leaching from agricultural lands provokes phosphate eutrophication in groundwater fed wetlands: the sulphur bridge. Biogeochemistry 98 (1–3), 1–7.
Soares, M.I.M., 2000. Biological denitrification of groundwater. Water Air Soil Pollut. 123 (1–4), 183–193.
Soto, D.X., Koehler, G., Wassenaar, L.I., Hobson, K.A., 2019. Spatio-temporal variation of nitrate sources to Lake Winnipeg using N and O isotope (δ15N, δ18O) analyses. Sci. Total Environ. 647, 486–493.
Stock, B.C., Semmens, B.X., 2016. Unifying error structures in commonly used biotracer mixing models. Ecology 97 (10), 2562–2569.
Strebel, O., Böttcher, J., Fritz, P., 1990. Use of isotope fractionation of sulfate-sulfur and sulfate-oxygen to assess bacterial desulfurication in a sandy aquifer. J. Hydrol. 121 (1–4), 155–172.
Stumm, W., Morgan, J.J., 1981. Aquatic chemistry.: an Introduction Emphasizing Chemical Equilibria in Natural Waters. Wiley, New York.
Toth, J., 1963. A theoretical analysis of groundwater flow in small drainage basins. J. Geophys. Res. 68 (16), 4795–4812.
Toth, J., 1970. A conceptual model of the groundwater regime and the hydrogeologic environment. J. Hydrol. 10 (2), 164–176.
Urresti-Estala, B., Vadillo-Pérez, I., Jiménez-Gavilán, P., Soler, A., Sánchez-García, D., Carrasco-Cantos, F., 2015. Application of stable isotopes (δ34S-SO4, δ18O-SO4, δ15N-NO3, δ18O-NO3) to determine natural background and contamination sources in the Guadalhorce River Basin (southern Spain). Sci. Total Environ. 506, 46–57.
Valiente, N., Carrey, R., Otero, N., Gutiérrez-Villanueva, M.A., Soler, A., Sanz, D., Castaño, S., Gómez-Alday, J.J., 2017. Tracing sulfate recycling in the hypersaline Pétrola Lake (SE Spain): a combined isotopic and microbiological approach. Chem. Geol. 473, 74–89.
Valiente, N., Carrey, R., Otero, N., Soler, A., Sanz, D., Muñoz-Martín, A., Jirsa, F., Wanek, W., Gómez-Alday, J.J., 2018. A multi-isotopic approach to investigate the influence of land use on nitrate removal in a highly saline lake-aquifer system. Sci. Total Environ. 631, 649–659.
Vera, J.A., Martín-Algarra, A., 2004. Cordillera bética. In: Vera, J.A. (Ed.), Geología de España. IGME-SGE, Madrid, pp. 345–464.
Vitòria, L., Otero, N., Soler, A., Canals, À., 2004. Fertilizer characterization: isotopic data (N, S, O, C, and Sr). Environ. Sci. Technol. 38 (12), 3254–3262.
Vitòria, L., Soler, A., Aravena, R., Canals, A., 2005. Multi-isotopic approach (15 N, 13 C, 34 S, 18 O and D) for tracing agriculture contamination in groundwater. Environmental Chemistry. Springer, Berlin, Heidelberg, pp. 43–56.
Vogel, J.C., Ehhalt, D., 1963. The use of the carbon isotopes in groundwater studies. In: Radioisotopes in Hydrology. Proceedings of a Symposium.
Ward, M.H., DeKok, T.M., Levallois, P., Brender, J., Gulis, G., Nolan, B.T., VanDerslice, J., 2005. Workgroup report: drinking-water nitrate and health—recent findings and research needs. Environ. Health Perspect. 113 (11), 1607–1614.
Wigley, T.M.L., 1973. The incongruent solution of dolomite. Geochem. Cosmochim. Acta 37 (5), 1397–1402.
Williams, W.D., 2002. Environmental threats to salt lakes and the likely status of inland saline ecosystems in 2025. Environ. Conserv. 29, 154–167.
Wunderlich, A., Meckenstock, R.U., Einsiedl, F., 2013. A mixture of nitrite-oxidizing and denitrifying microorganisms affects the δ18O of dissolved nitrate during anaerobic microbial denitrification depending on the δ18O of ambient water. Geochem. Cosmochim. Acta 119, 31–45.
Wurtsbaugh, W.A., Miller, C., Null, S.E., DeRose, R.J., Wilcock, P., Hahnenberger, M., Howe, F., Moore, J., 2017. Decline of the world's saline lakes. Nat. Geosci. 10 (11), 816.
Yue, F.J., Li, S.L., Liu, C.Q., Lang, Y.C., Ding, H., 2015. Sources and transport of nitrate constrained by the isotopic technique in a karst catchment: an example from Southwest China. Hydrol. Process. 29 (8), 1883–1893.